Available online at www.sciencedirect.com
ScienceDirect
Journal of the European Ceramic Society 31 (2011) 2559–2568
www.elsevier.com/locate/jeurceramsoc

Preparation of ceramic nanospheres by CO_2 laser vaporization (LAVA)

Heinz-Dieter Kurland *, Janet Grabow, Frank A. Müller

Friedrich-Schiller-University of Jena, Institute of Materials Science and Technology (IMT), Löbdergraben 32, 07743 Jena, Germany

Available online 12 February 2011

Abstract

In order to prepare ceramic nanoparticles by CO_2 laser vaporization (LAVA) coarse ceramic powders (e.g. ZrO_2, Al_2O_3, and TiO_2) were used as raw materials. The raw powder was vaporized into a flowing process gas under normal pressure. Expanding into the gas, the vapor instantly cools down. Gas-phase condensation leads to the formation of nanoscale particles with a composition that corresponds to that of the raw powder. LAVA nanoparticles are chemically pure, spherical, crystalline, exhibit a narrow size distribution, and form merely soft agglomerates. The co-laser vaporization of mixtures of ceramic raw powders allows for the preparation of nanoparticles of multi-phase (e.g. Fe_2O_3–SiO_2) or single-phase (e.g. $CaTiO_3$) mixed-oxides and dispersion ceramics (e.g. ZrO_2–Al_2O_3). In order to modify the surface of the nanoparticles they can be coated in-process with an organic additive. Thus, the LAVA method allows for the targeted development of a wide range of ceramic nanopowders with tailored properties.

Keywords: Laser vaporization; Nanocomposites; ZrO_2; Al_2O_3; TiO_2

1. Introduction

Nowadays the global industrial competition is increasingly determined by the development of a new class of materials that allows the fabrication and application of novel products with optimized or even totally new properties. Many of these developments and products base on ultra-fine ceramic powders with grain sizes of only a few nanometers. These nanoscaled particles are characterized by a high surface-to-volume ratio, i.e. a large fraction of surface atoms. This might lead to physical and chemical properties which distinctly differ from those of the same material at larger scale. Properties related to the particle size include sintering activity, catalytical activity, photoactivity, and bioactivity, to name only a few. The unique properties of nanoscaled particles strongly depend on their shape, size, surface characteristics, and inner structure. Thus, composite nanoparticles with even smaller characteristic sizes of the intraparticular domains will enable the design of materials with further enhanced physical and chemical properties. Due to the outstanding potential of ultra-fine particles various technologies for their preparation were intensively investigated, including sol–gel technologies,[1,2] wet chemical precipitation,[3,4] flame processes,[5–7] or laser ablation.[8–11] The challenge to be met now is to adapt their properties, qualities, and quantities to the requirements of individual and new applications.

Here, we give an overview of the preparation of ceramic nanoparticles by a particular laser vaporization (LAVA) process.[12–14] This highly versatile and potent method allows for the continuous production of a wide variety of nanoscaled particles and nanopowders under well defined and stable conditions. A broad spectrum of various materials, including ceramic and composite nanopowders,[15–18] is procurable, since there is no need for particularly designed precursors. Unlike wet chemical preparation routes, e.g. the sol–gel method, organic solvents which would require a drying process are not involved.

2. Materials and methods

2.1. LAVA principle and laboratory setup

For the preparation of nanoscaled ceramic particles with the LAVA process coarse ceramic powders with grain sizes ranging from μm to mm are used as raw materials. Generally their chemical composition is the same as that of the target nanopowders. In order to vaporize the provided raw powder a laser beam is focused onto its surface (Fig. 1). Absorbing the high-intensity laser radiation within the beam focus, the raw material heats up, vaporizes, and forms a plasma. Vaporization and plasma for-

* Corresponding author. Tel.: +49 3641 947762; fax: +49 3641 947702.
E-mail address: H.D.Kurland@gmx.net (H.-D. Kurland).

0955-2219/$ – see front matter © 2011 Elsevier Ltd. All rights reserved.
doi:10.1016/j.jeurceramsoc.2011.01.010

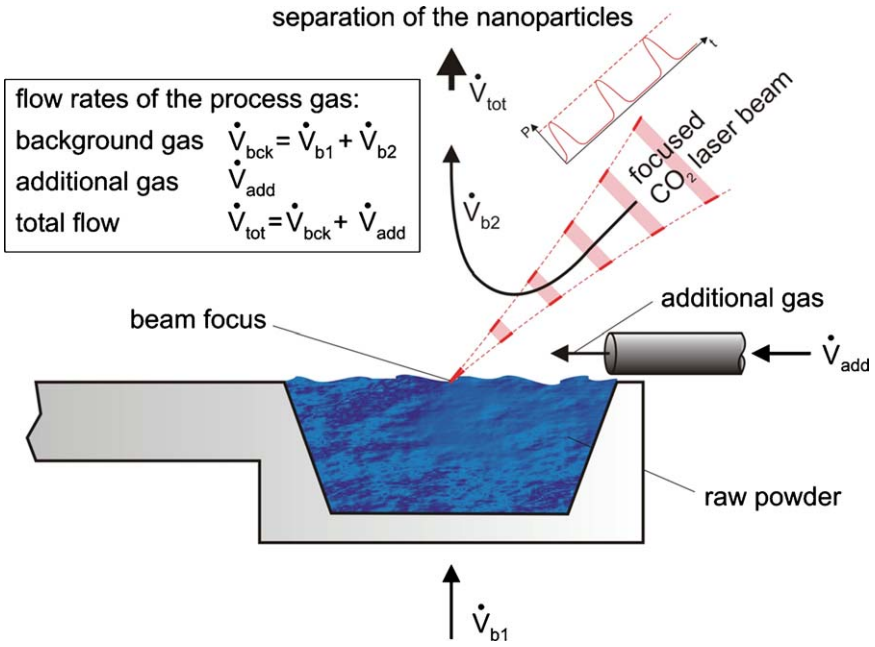

Fig. 1. Principle of the laser vaporization process.

mation proceed in a continuously flowing aggregation (process) gas under normal pressure. For the processing of oxidic ceramic materials air is used as process gas. During expansion into the flowing aggregation gas, plasma and vapor instantly cool down. Subsequently, gas phase condensation leads to the formation of an ultra-fine particle aerosol. Finally, the process gas transports the resulting aerosol towards the particle separation.

This principle of function was implemented in the LAVA laboratory system (Fig. 2, Table 1) which allows the continuous production of nanopowders under well defined and stable process conditions. In order to achieve high vaporization rates (mass of vaporized raw material per time unit), a high-power CO_2 laser was chosen as the beam source. The CO_2 laser radiation in the middle infrared part of the electromagnetic spectrum is absorbed to a high degree by the ceramic raw materials. The laser can be operated in a continuous beam mode as well as in a variable pulsed mode. Vaporization and particle formation proceed in a stainless-steel chamber. The main part of the vaporization chamber is a motor-driven revolvable disc (maximum rotational frequency 15 rpm) with a ring-shaped channel along its rim. The ceramic raw powder is filled into this channel. The CO_2 laser beam is focused onto the continuously revolving powder surface through an inlet tube in the chamber and vaporizes the raw powder. During the rotation of the disc, the vaporized material is automatically refilled by a variable powder doser. A doctor blade continuously planishes the surface of the refilled powder. Thereby, an incessantly regenerated powder surface is fed to the focus of the laser beam, ensuring stable and reproducible process conditions. The vaporization chamber is connected to the filtering chamber through a system of hermetically sealed glass tubes.

Table 1
Technical data of the LAVA laboratory system.

CO_2 laser type	FEHA SM 2000E (Feinmechanische Werke Halle, Germany), maximum continuous power up to $P_{max} = 2$ kW, wavelength $\lambda = 10.59$ μm, electrically pulsable
Focusing mirror	Focal length $f = 1000$ mm, focus intensity up to $I_{max} = 0.15$ MW/cm^2
Process gas	Air or gas mixtures, total volume flow rate up to $\dot{V}_{tot} = 20$ m^3/h, flow rate of the additional gas up to $\dot{V}_{add} = 6$ m^3/h
Powder separation	Paper filter tube
Production rates	Dependent on material and process parameters up to several 10 g/h

The total flow rate of the process gas $\dot{V}_{tot}$ is comprised of two variable gas flows (Fig. 1), the background gas flow (flow rate $\dot{V}_{bck}$) through the evaporation chamber that is provided by a gas extraction fan and an additional jet of gas (flow rate $\dot{V}_{add}$) that is conducted through the zone of particle condensation. The process gas flow transports the nanoparticles out of the vaporization chamber towards the filtering chamber where they are separated from the aerosol by a filtering unit. During the process of vaporization, the transmission of the filter continuously decreases due to the accumulation of nanopowder on its surface. In order to keep the process gas flow constant, the power of the gas extraction fan has to be adjusted. For this purpose the differential pressure between the filtering chamber and the ambient laboratory atmosphere is used as a control. Once the maximum power of the fan is achieved, the filter is regenerated by mechanically stripping off the nanopowder.

The LAVA process and thereby the quality of the ceramic nanopowders is controlled by the relevant process parameters laser power, continuous or pulsed laser operation, and also volume flow and thermal conductivity of the process gas within the zone of particle condensation. To allow for a further customization or conditioning of the laser-generated nanoparticles, the basic process can be varied or supplemented by the co-laser

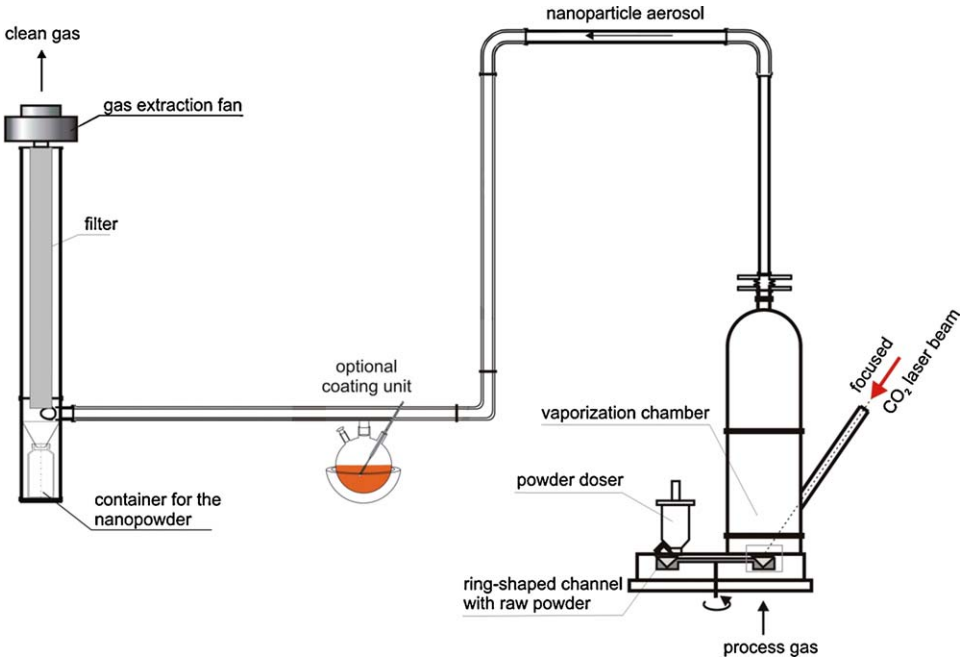

Fig. 2. Schematic representation of the LAVA laboratory system.

vaporization (CoLAVA) method or the in-process coating of the aerosol particles, respectively.

2.2. Co-laser vaporization

The CoLAVA method is used to achieve multi-phase or single-phase mixed-oxide nanoparticles. For this purpose homogeneous mixtures of at least two ceramic raw powders are co-laser evaporated in one single process (Fig. 3). Starting from a mixture of several oxides the composition of the resulting nanoparticles depends on the thermal behavior of the raw components, their reactivity within the mixture as well as on their mixing ratios. In general the components of the raw mixture have different rates of vaporization. Therefore it is not possible to map the mixing ratio of the raw components onto the phase composition of the resulting nanoparticles. To obtain defined phase ratios in the nanopowder, the mixing ratio of the raw powders has to be determined experimentally. In order to prevent the depletion of the component with the higher vaporization rate in the raw mixtures, fresh mixtures have to be supplied continuously during the co-vaporization process.

2.3. In-process coating

The in-process coating of the airborne nanoparticles was developed in order to homogeneously introduce additives into the ceramic nanopowders or to protect sensitive nanoparticles from oxidation or hydrolysis.[19] For this purpose, the particle aerosol is led through a supersaturated vapor atmosphere of the additive component (Fig. 4) before the aerosol reaches the filtering chamber. The ultrafine airborne particles act as condensation

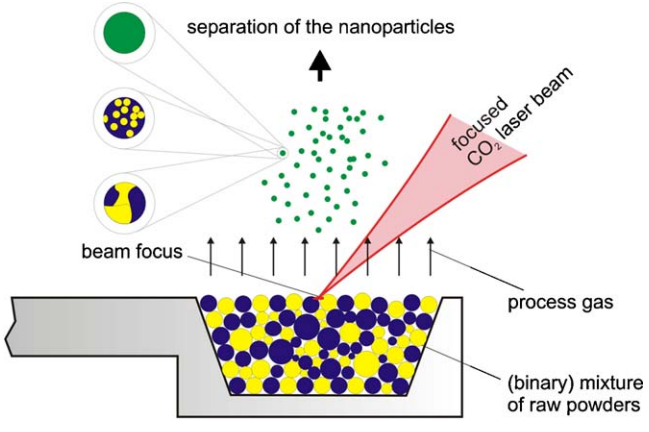

Fig. 3. Principle of the co-laser vaporization process.

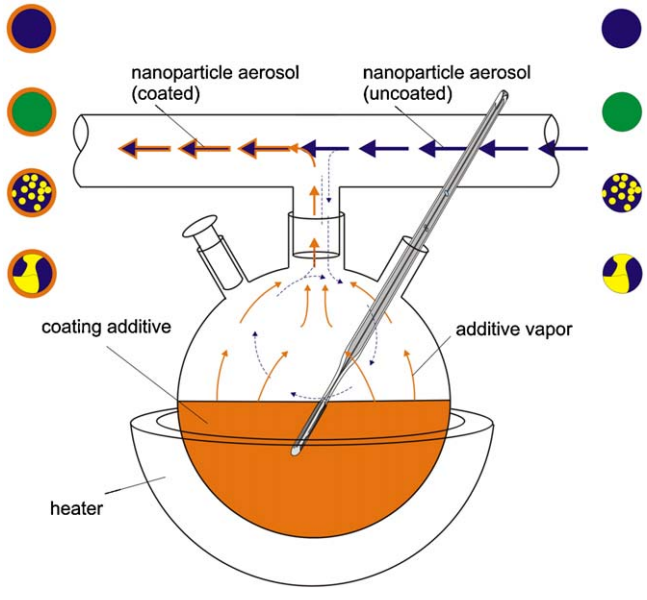

Fig. 4. Principle of the in-process particle coating procedure.

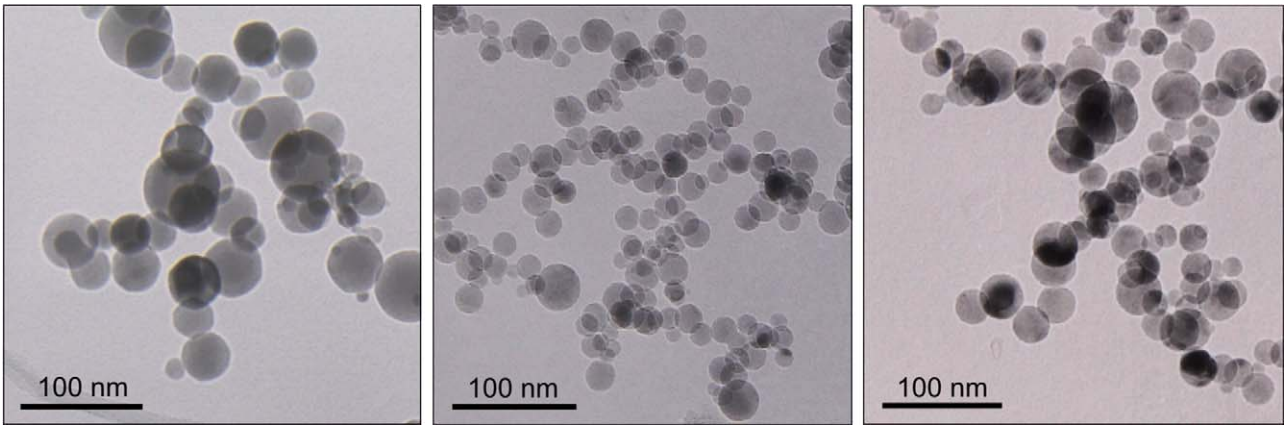

Fig. 5. TEM micrographs of LAVA prepared ZrO_2, Al_2O_3, and TiO_2 nanoparticles (from left to right) applying continuous laser radiation.

site so that the additive forms a layer on the aerosol particles by heterogeneous nucleation. The additive is evaporated by a downstream heating unit (maximum temperature 300 °C) which is coupled with the glass tube system (Fig. 2). The coating thickness and thereby the portion of the additive can be adjusted by its temperature, i.e. by its vapor pressure. In order to support the condensation process, the temperature difference between the additive vapor and the particles should be as high as possible. To achieve this, the particle aerosol can be quenched with additional process gas which has been cooled down in a cryostat with liquid nitrogen before it reaches the coating unit. Suitable additives have to be solid at room temperature and must be capable of being evaporated without decomposition.

3. Results and discussion

3.1. Ceramic nanoparticles derived from the basic LAVA process

The LAVA method allows for the production of a wide range of ceramic nanopowders. Zirconium dioxide (zirconia, ZrO_2), aluminum oxide (alumina, Al_2O_3) and titanium dioxide (tita-

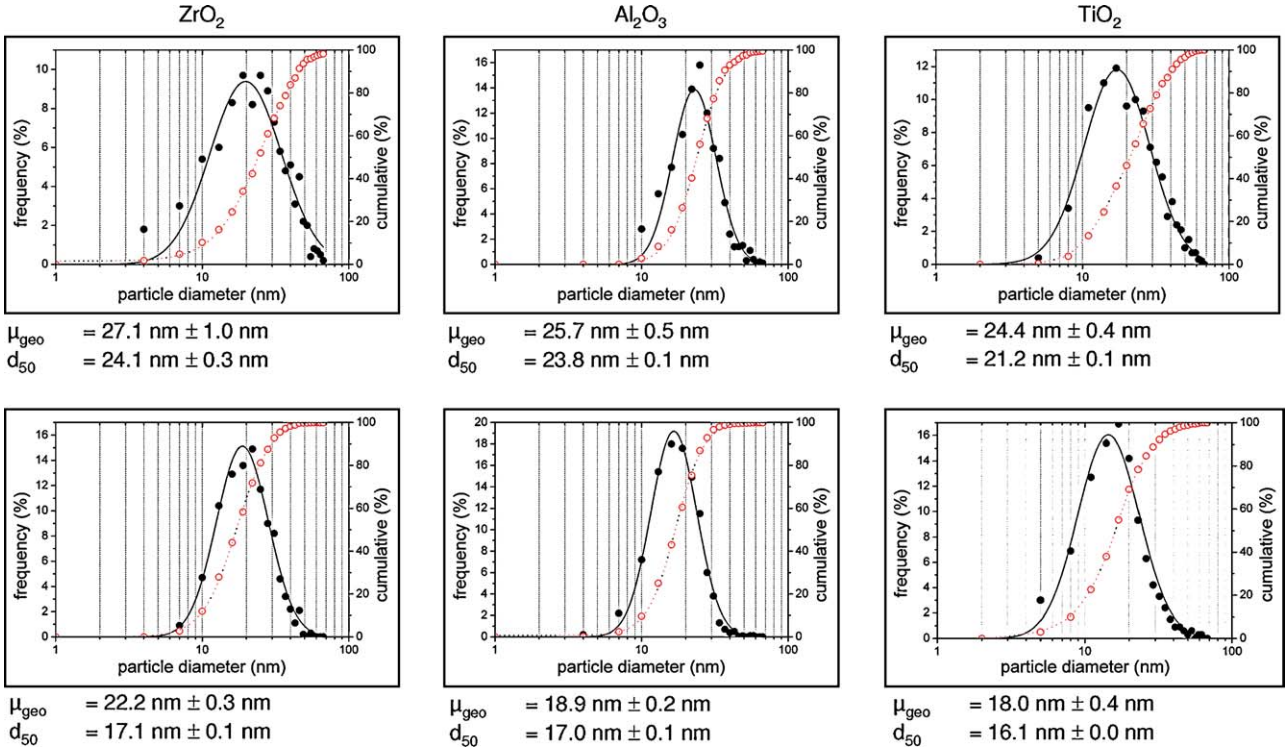

Fig. 6. Particle diameter distributions of the LAVA prepared ZrO_2, Al_2O_3, and TiO_2 nanopowders (from left to right) applying continuous (upper row) and pulsed laser radiation (lower row): density (—, ●) and cumulative distributions (. . ., ○) on number basis, geometric mean values μ_{geo} and d_{50} values (50% of the particles have smaller diameters than this value) of the particle diameters. Process conditions for the preparation of the ZrO_2, Al_2O_3, and TiO_2 samples using the continuous laser mode: $P = 2$ kW, $\dot{V}_{add} = 2\ m^3/h$, process conditions for the preparation of the ZrO_2 and Al_2O_3 samples using the pulsed laser mode: $\tau = 1$ ms, $f = 200$ Hz, $\hat{P} = 2$ kW, $\bar{P} = 735$ W, $\dot{V}_{add} = 2\ m^3/h$, and for the preparation of the TiO_2 sample using the pulsed laser mode: $\tau = 500$ μs, $f = 100$ Hz, $\hat{P} = 2$ kW, $\bar{P} = 100$ W, $\dot{V}_{add} = 4\ m^3/h$.

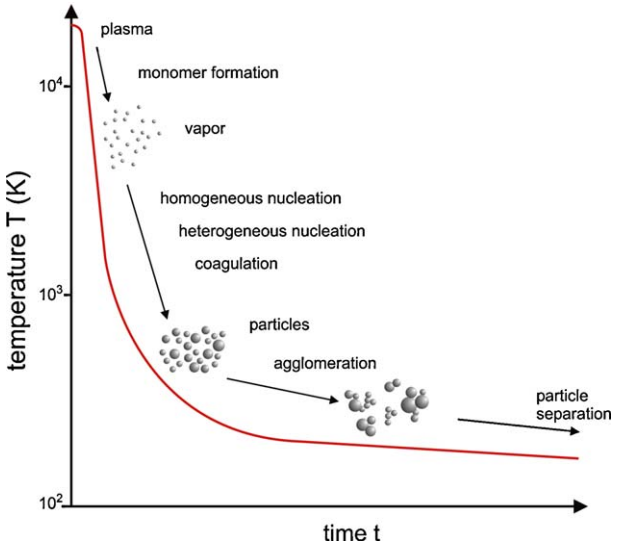

Fig. 7. Time-temperature dependent stages of particle formation within the LAVA process.
Adapted from Ullmann et al.[10]

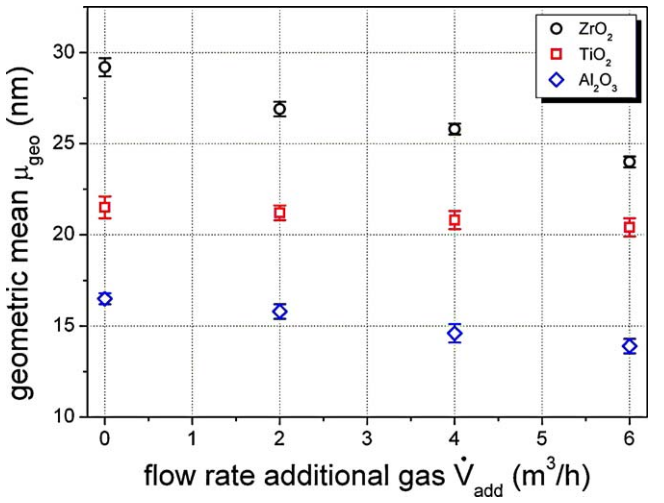

Fig. 8. Geometric mean diameters μ_{geo} of the LAVA prepared ZrO_2, Al_2O_3, and TiO_2 nanoparticles at varied flow rates $\dot{V}_{add}$ of the additional gas jet. Constant process conditions applied for the preparation of all samples: pulsed laser radiation with $\tau = 500\,\mu s$, $f = 200\,Hz$, and $\bar{P} = 200\,W$.

nia, TiO_2) were selected to discuss the particle formation and the characteristic features of single phase, unmodified LAVA nanopowders. As raw powders for the laser vaporization corundum (α-Al_2O_3, Alcoa, A16SG), yttrium stabilized tetragonal zirconia (ZrO_2, Tosoh Corp., TZP-3Y) and anatase (TiO_2, VWR BDH Prolabo, GPR Rectapur 20732.298) were used. These raw materials were vaporized under air applying a continuous laser radiation with the maximum power of $P = 2\,kW$ and an additional air jet through the nucleation zone. Production rates of 27 g, 24 g, and 17 g nanopowder per hour were achieved, respectively. Transmission electron microscopic (TEM) micrographs reveal the typical morphology of LAVA generated ceramic nanoparticles (Fig. 5). The density and cumulative particle diameter distributions of these three powder samples were derived from statistical TEM analysis (Fig. 6, upper row). The particle diameters show unimodal log-normal distributions.

The nanoscaled particles are of spherical shape and merely softly agglomerated by weak van der Waals forces. Only a marginal fraction of particles is firmly bonded by solid state bridges (sinter necks). These findings reflect the LAVA principle (Fig. 7): starting with the evaporation of the ceramic raw powder into a plasma particle formation proceeds through various time-temperature dependent stages.[10] The plasma components expand into the flowing carrier gas forming "monomers". Within the resulting supersaturated vapor these monomers collide and build growing clusters by homogeneous nucleation. The emerging clusters act as nuclei for the condensation of the vapor and melt droplets arise by heterogeneous nucleation. The growth of the droplets proceeds by surface condensation and by coagulation. With falling temperature condensation and coagulation cease, and the size of the primary particles is set by the solidification of the droplets. Further collision of the primary particles leads to the formation of chain-like or flocculent agglomerates. Hereby the particles can adhere to each other by weak forces, i.e. van der Waals, magnetic or Coulomb forces, forming soft agglomerates or by sinter necks, forming hard agglomerates. The latter are formed, if particles collide at temperatures above the concerning temperature of solidification. Thus, they might meld at their contact point without forming a spherical particle. In all these sub-processes of particle formation, i.e. growth of the condensation nuclei, growth of the melt droplets, and growth of the agglomerates, the probability of collision between the involved components plays a crucial role.[20] The probability and thus the rate of collision decreases with decreasing kinetic energy, with decreasing volume concentration, and with decreasing collision cross-section of the involved components. The sizes of the primary particles and of their agglomerates can thus be influenced by the cooling rate and the volume concentration of the components within the zone of condensation.[13,21,15]

Driven by the process gas flow the components of the interaction zone run through a steep temperature gradient between the hot evaporation zone and the surrounding atmosphere. The rapid quenching considerably accelerates nucleation, condensation, coagulation, and solidification. Hence, the time of life of liquid particles is very limited and impedes their growth by coagulation. Therefore, only nanoscaled primary particles with diameters below 100 nm arise. Additionally, the continuous volume flow of the carrier gas reduces the volume concentration of droplets and hot particles. Thereby the probability of collision is significantly reduced and hard agglomeration by edge melting or sintering is suppressed to a large extent.

Although LAVA generated nanoparticles usually are crystalline they exhibit an almost spherical morphology. Crystal habits are determined by the symmetry of the accordant crystal system as long as the crystal growth proceeds under equilibrium conditions. Within the LAVA process, however, the hot melt droplets emerging in the zone of condensation are rapidly quenched to a solid state. Their crystallization thus proceeds under nonequilibrium conditions where the mobility of the atomic components is significantly reduced and the minimization of the crystallite's surface energy is impeded.

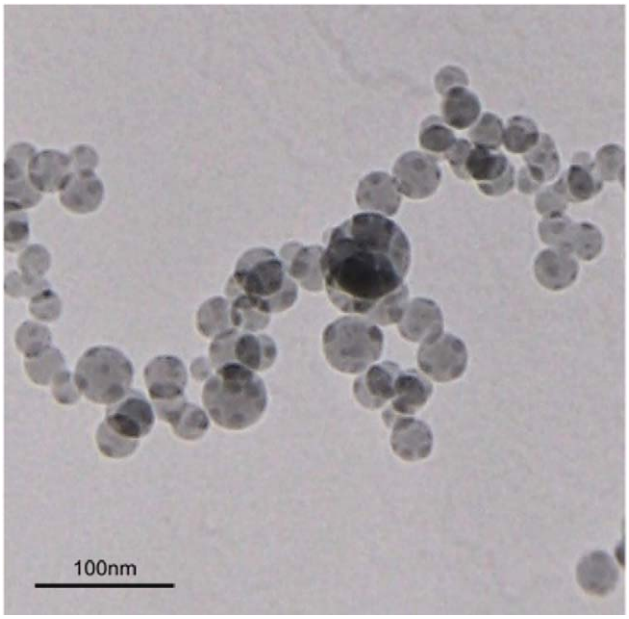

Fig. 9. TEM micrograph of Fe_xO_y nanocrystallites embedded in a silica glass matrix yielded by the co-laser vaporization of the mixture of α-Fe_2O_3 and SiO_2.

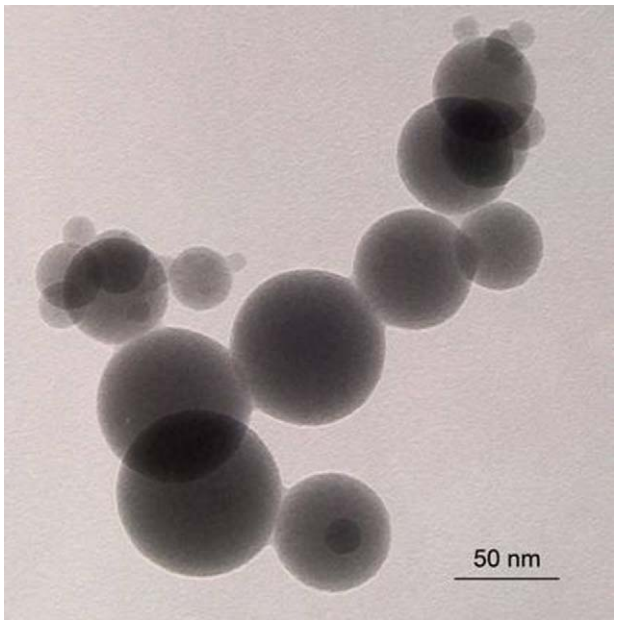

Fig. 10. TEM micrograph of nanoparticles yielded by the co-laser vaporization of the mixture of TiO_2 and CaO.

Most of the ceramic raw materials exist in different polymorphs. Even under the extreme conditions, i.e. plasma temperatures, within the evaporation zone, the LAVA process commonly yields the low temperature polymorphs. Obviously the polymorphic systems follow Ostwald's rule of stages[22,23] which states that upon cooling a multi-phase system will pass stepwise through all the metastable phases before reaching the thermodynamically most stable state. According to the Ostwald–Volmer rule the less dense phase forms at first.[24,25] Related to the titania system this means: the crystallization of the melt droplets initially yields anatase (density $\rho = 3.84\ g/cm^3$).[26] Within the LAVA process the quenching of the emerging anatase particles proceeds very fast and far away from equilibrium conditions. Due to the short time interval, within which the temperature of the anatase particles is above the transition threshold at about 700 °C,[27] virtually no rutile ($\rho = 4.26\ g/cm^3$)[26] can arise and the anatase structure is literally frozen. The same applies for alumina: here the crystallization of the melt droplets yield γ-Al_2O_3 as the major phase and other transition alumina (e.g. δ- or ε-Al_2O_3) as the minor phases with densities of up to $3.65\ g/cm^3$.[28] Also in the case of alumina the cooling down of the crystallized particles proceeds so fast, that the transition alumina particles cannot transfer to the high temperature polymorph, α-Al_2O_3 (transition threshold about 1000 °C).[28] For both titania and alumina these findings are independent from the crystal structures of the supplied raw materials. Different is the case if TZP-3Y is laser vaporized. Herein the tetragonal structure of ZrO_2 is stabilized by the addition of 3 mol% of yttria (Y_2O_3). The presence of Y_2O_3 prevents the formation of monoclinic ZrO_2 (density of undoped monoclinic ZrO_2, $\rho = 5.6\ g/cm^3$),[29] the low temperature polymorph. Instead the droplets crystallize in the tetragonal structure (density of undoped tetragonal ZrO_2 $\rho = 6.1\ g/cm^3$)[29] still containing the Y_2O_3 dopand. But again, due to the rapid quenching the tetragonal ZrO_2 particles cannot transfer to cubic ZrO_2 (density of undoped cubic ZrO_2 $\rho = 6.27\ g/cm^3$,[29] transition threshold about 2350 °C),[29] the high temperature polymorph.

For a given raw material the production rates of the LAVA process depend on the applied power of the CO_2 laser radiation, i.e. on the radiation intensity in the interaction zone. Different laser regimes and gas flow rates $\dot{V}_{add}$ however indicate a significant impact on the particle sizes. Applying a pulsed laser radiation (Fig. 6, lower row) and an increased gas flow rate (Fig. 8) causes smaller primary particles in comparison to the usage of a continuous radiation (Fig. 6, upper row) and a lower gas flow rate due to an accelerated cooling of the particles. Additionally, the volume concentrations of the vapor and of the emerging droplets are reduced. Thus, smaller droplets arise due to the retarded growth by surface condensation and due to the reduced probability for coagulation processes.

3.2. Ceramic nanoparticles derived from the CoLAVA process

The co-laser vaporization of homogeneous mixtures of raw powders can result in different intraparticular phase distributions and different morphological sub-structures of the resulting nanoparticles.

One option of the CoLAVA process is that nano-composites are formed in which nanocrystallites are embedded in a nanoscaled glass matrix. For this purpose a mixture of a glass former and the component which shall be embedded has to be co-laser vaporized. Exemplified we used this method to obtain nanoparticles consisting of magnetic iron oxide nanoparticles embedded in a nanoscaled silica (SiO_2) matrix.[18] For this purpose, a homogeneous mixture of coarse hematite (α-Fe_2O_3, Aldrich) and SiO_2 powders (quartz sand) with a mass ratio α-Fe_2O_3:SiO_2 of 1:1.5 was prepared. This mixture was

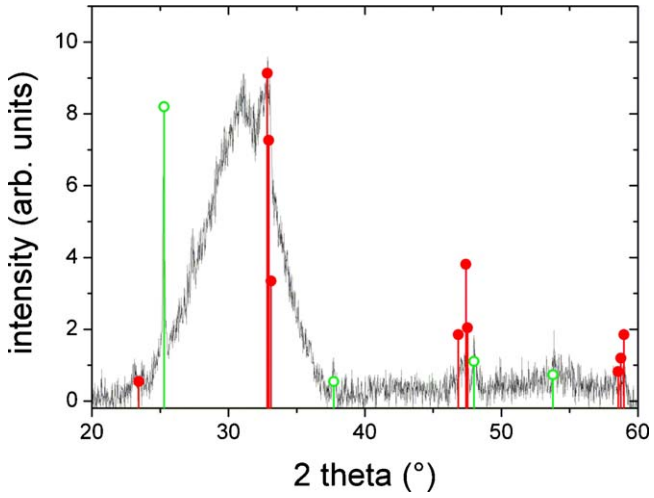

Fig. 11. XRD diagram of the nanopowder yielded by the co-laser vaporization of the mixture of TiO_2 and CaO. The reference XRD data for anatase (TiO_2, ○) and perovskite ($CaTiO_3$, ●) were taken from the database of the Joint Committee on Powder Diffraction Standards (JCPDS).

vaporized applying pulsed laser radiation (pulse length $\tau = 1$ ms, repetition frequency $f = 200$ Hz, peak power $\hat{P} = 2$ kW, mean power $\bar{P} = 710$ W) using air as background process gas ($\dot{V}_{bck} = 12.5\ m^3/h$). In order to minimize the nonmagnetic hematite content of the processed powders, an additional anoxic gas jet (nitrogen, $\dot{V}_{add} = 2\ m^3/h$) was led through the nucleation zone.[17] The resulting nanopowder contained only the magnetic phases maghemite (γ-Fe_2O_3) and magnetite (Fe_3O_4) together with amorphous silica. TEM micrographs (Fig. 9) of the resulting spherical Fe_xO_y-SiO_2 composite powder predominantly display small, spherical, and isolated iron oxide nanoparticles which are embedded in a brighter silica matrix. This can be explained by the nucleation process, in which the Fe_xO_y vapor condensates at first forming droplets and particles. Subsequently the SiO_2 vapor condensates on the surfaces of these iron oxide droplets or particles, inhibiting their further growth and embedding them within a silica glass matrix. A closer examination reveals that in the presence of SiO_2 the Fe_xO_y crystallite size does not exceed 20 nm, but remains mostly in the sub 10 nm range. Due to their small diameter the embedded particles show superparamagnetic behavior.[18] In contrast, iron oxide nanoparticles prepared under the same LAVA process conditions but without SiO_2 grow to larger diameters (refer to Fig. 14) and exhibit ferromagnetic behavior.[17]

A second option is the formation of mixed-oxide, solid solution nanoparticles. For their preparation a mixture of raw components which are soluble in each other has to be co-laser vaporized. An example is the binary mixture of CaO (calcium oxide) and TiO_2. The co-vaporization and co-condensation of equimolar amounts of the single components should result in single phase perovskite ($CaTiO_3$) nanoparticles. Applying pulsed laser radiation ($\tau = 500$ μs, $f = 100$ Hz, $\hat{P} = 2$ kW, $\bar{P} = 100$ W) CaO (VWR Prolabo, 22645.360) and TiO_2 (anatase, VWR Prolabo, 20732.298) exhibit different vaporization rates of 1.47 g/h (0.026 mol/h) and 1.25 g/h (0.016 mol/h), respectively. With the objective to co-vaporize equimolar amounts of CaO and TiO_2

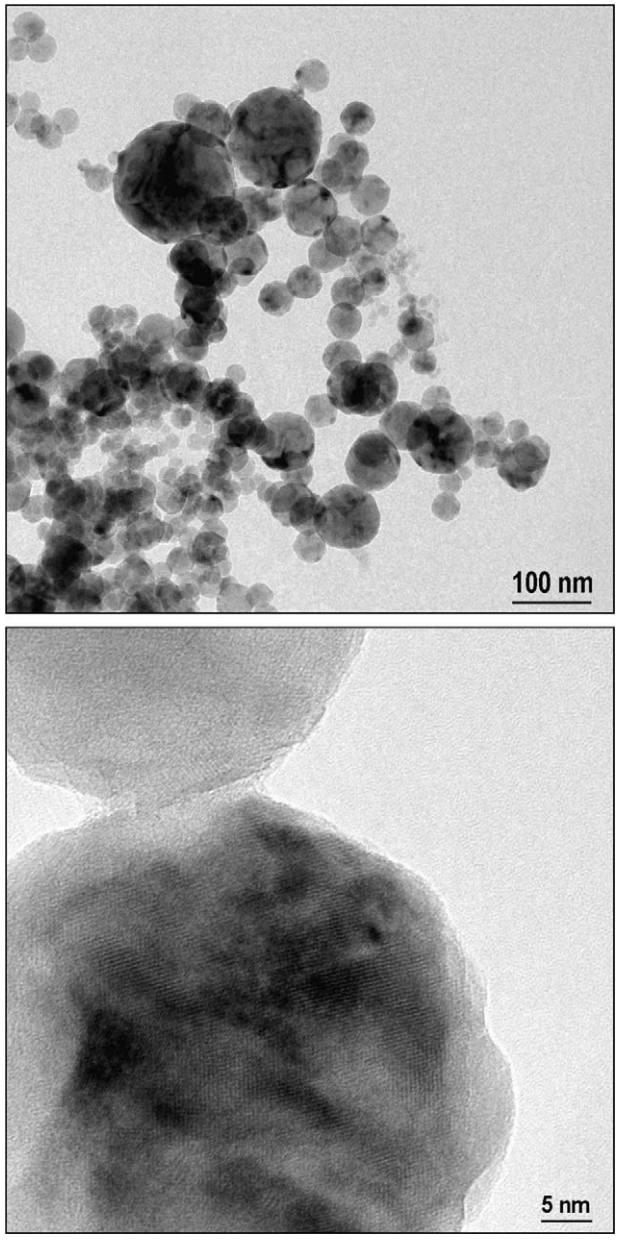

Fig. 12. TEM micrographs of nanoparticles yielded by the co-laser vaporization of the mixture of ZrO_2 and Al_2O_3.

and considering the different vaporization rates the raw mixture was prepared with a molar CaO:TiO_2 ratio of 0.60:1 (according to a mass ratio of 0.42:1). Applying the aforementioned laser regime this mixture was co-vaporized using air as process gas $\dot{V}_{tot} = 14.5\ m^3/h$. TEM micrographs (Fig. 10) reveal the spherical shape of the resulting nanoparticles and their tendency to form undesirable interparticular solid state bridges (sinter necks). On this scale intraparticular phase boundaries are not observable. In the according X-ray diffraction (XRD) diagram (Fig. 11) two crystal phases, perovskite and anatase, can be identified. Despite of this promising result regarding the formation of the perovskite phase further experiments have to be performed which have to prove whether a reduction of TiO_2 in the raw mixture would lead to a pure perovskite nanopowder.

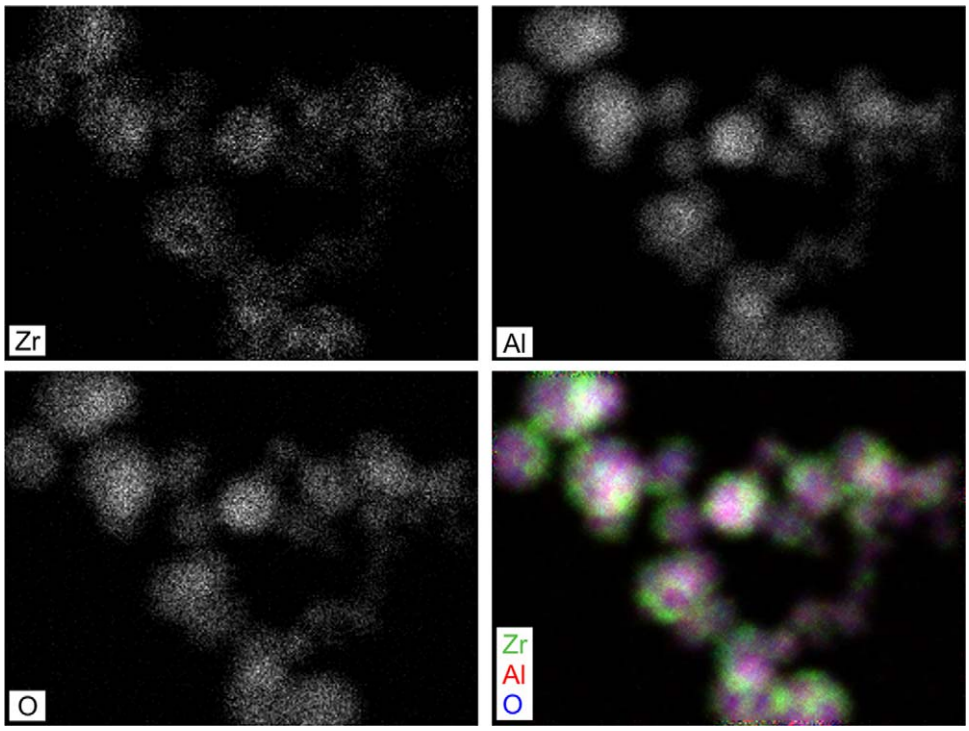

Fig. 13. EDX elemental dot maps for zirconium (Zr), aluminum (Al), and oxygen (O) of nanoparticles yielded by the co-laser vaporization of the mixture of ZrO_2 and Al_2O_3.

The third option is the formation of composite nanoparticles consisting of different crystalline phases. These particles can result from the co-vaporization of components which exhibit only very limited mutual solubility and thus forming an intraparticular dispersion. Prominent representatives of such materials are the dispersion ceramics alumina toughened zirconia (ATZ) and zirconia toughened alumina (ZTA).[30–32] Here, the CoLAVA procedure can be used to produce nanoparticles with an intraparticular dispersion of zirconia and alumina. The raw mixture was prepared from coarse powders of yttrium stabilized tetragonal zirconia (Tosoh Corp., TZP-3Y) and corundum (Alcoa, A16SG) in a mass ratio of 1:0.45 according to a phase composition of 62.5 mol% (63.8 wt.%) ZrO_2, 36.0 mol% (30.5 wt.%) Al_2O_3, and 1.6 mol% (2.9 wt.%) Y_2O_3. This starting mixture was co-vaporized using continuous laser radiation ($P = 2$ kW) and air as process gas ($\dot{V}_{tot} = 14.5$ m^3/h). The XRD diagram of the resulting nanopowder indicated the presence of two crystal phases, tetragonal ZrO_2 and the transition alumina δ-Al_2O_3. There was no hint for the occurrence of aluminum–yttrium compounds. The chemical analysis using inductively coupled plasma optical emission spectrometry (ICP-OES) revealed the following composition: 40.1 mol% (42.9 wt.%) ZrO_2, 59.3 mol% (52.5 wt.%) Al_2O_3, and 0.6 mol% (1.1 wt.%) Y_2O_3. The discrepancy in the composition of the starting mixture and the resulting nanopowder is due to the different vaporization rates of the components. The mean crystallite sizes of the tetragonal ZrO_2 and the δ-Al_2O_3 were determined from the XRD pattern (refined by Rietveld analysis). They amounted to 11 nm and 6 nm, respectively. TEM micrographs (Fig. 12) show approximately spherical nanoparticles with distinct inner structures. The element mapping applying energy dispersive X-ray (EDX) spectroscopy indicates that separated crystalline domains of ZrO_2 and Al_2O_3 coexist within the nanoparticles (Fig. 13).

3.3. In-process coated ceramic nanoparticles

The in-process particle coating is illustrated with iron oxide (Fig. 14) and titania nanoparticles (Fig. 15) coated with a layer of stearic acid ($C_{18}H_{36}O_2$, Merck KGAA, purity ≥ 95%, melting point 65–68 °C, boiling point 370 °C). The iron oxide nanoparticles were prepared starting from a coarse hematite powder (α-Fe_2O_3, Aldrich) which was vaporized using pulsed laser radiation ($\tau = 1$ ms, $f = 200$ Hz, $\hat{P} = 2$ kW, $\bar{P} = 710$ W), air as background process gas, and an additional anoxic gas jet (nitrogen, $\dot{V}_{add} = 2$ m^3/h) in order to minimize the nonmagnetic hematite content in the prepared iron oxide nanopowder. The stearic acid was evaporated into the flowing particle aerosol at a temperature of 210 °C. Under these conditions uniform and dense layers of stearic acid were formed on the particles' surfaces with a mean thickness of 10 ± 3 nm.[18] The titania nanoparticles were prepared starting from a coarse anatase powder (TiO_2, VWR BDH Prolabo, GPR Rectapur 20732.298) which was vaporized applying continuous laser radiation ($P = 2$ kW) with air as background process gas and an additional gas jet ($\dot{V}_{add} = 2$ m^3/h) through the nucleation zone. The stearic acid was evaporated into the flowing particle aerosol at a temperature of 220 °C. Uniform and dense layers of stearic acid with a thickness of 5–6 nm were formed on the particles' surfaces.[15]

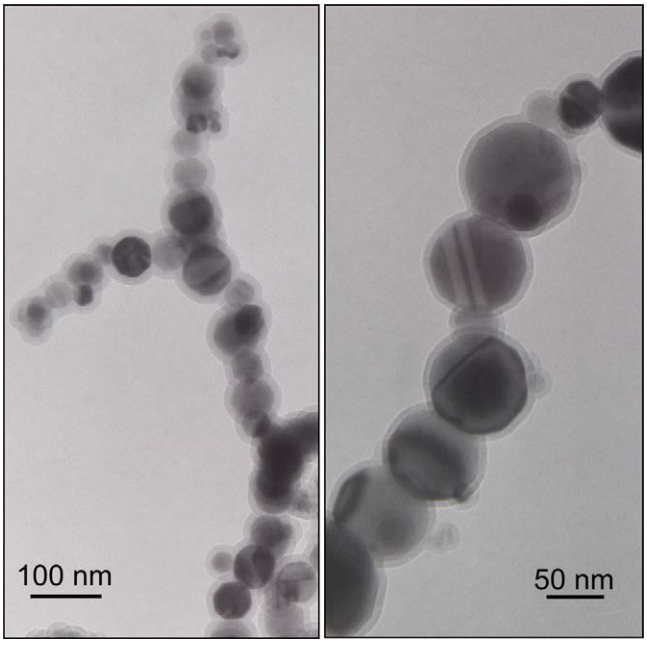

Fig. 14. TEM micrographs of Fe_xO_y nanoparticles prepared by laser vaporization and in-process coated with stearic acid.

In both cases the unavoidable soft agglomeration of the primary particles in the flowing aerosol due to magnetic and van der Waals forces prevents the complete coverage of individual nanoparticles with a uniform additive layer. Rather, the stearic acid coated entire agglomerates with a dense layer.[33] For a given nanopowder the layer thickness depends on the supersaturation of the additive vapor within the particle aerosol and the surface area of the particles which is available for the coating. The supersaturation can be controlled by the temperature of the additive, i.e. by its vapor pressure.[19] The available surface area depends on the vaporization rate of the raw powder and is controlled by the applied laser power.

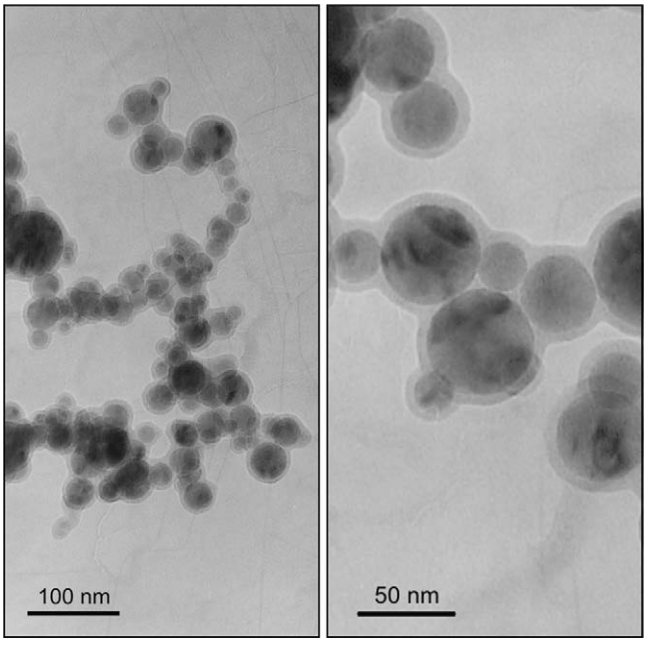

Fig. 15. TEM micrographs of TiO_2 nanoparticles prepared by laser vaporization and in-process coated with stearic acid.

Stearic acid was chosen as a coating additive not only because it might act as compacting aid during subsequent ceramic processing of the nanopowders. In-process generated layers of stearic acid have also been proven to protect hydrolysis-sensitive nanoparticles, e.g. aluminum nitride.[19] The only requirement for a successful in-process coating is that the chosen organic additive is capable of being evaporated without decomposition. For example, acrylic acid in the form of poly-acrylic acid might be used as coating additive in order to stabilize slurries of ceramic nanopowders. Aluminum isopropoxide as precursor for alumina might be used as coating additive. The post-process thermolysis of thus coated particles results in alumina-coated particles where the alumina layer acts as an inhibitor of grain growth in the sintering process of ceramic nanopowders.

4. Conclusions

The LAVA process proved to be a suitable method for the production of a wide range of oxidic ceramic nanopowders. Laser generated ceramic nanoparticles are spherically shaped and merely softly agglomerated by weak van der Waals forces. The mean particle size can be controlled by the rate of gas flow through the LAVA condensation zone and by the laser regime, i.e. by applying a continuous or a pulsed mode. In general, the raw powders and the produced nanopowders are of the same chemical composition. Accordingly, no especially designed precursors are required. Economic and widely available raw powders are processable. Achievable evaporation rates make it possible to prepare powder quantities sufficient for technical suitability tests. The characteristic properties of the LAVA nanoparticles are prerequisites in order to exploit their full potential concerning various surface active functionalities. The simultaneous vaporization of several powders of different compositions allows for the production of multi-phase or single-phase mixed-oxide nanoparticles with specific tailor-made properties. The in-process coating with an organic layer allows for the functionalization of the particles' surface to meet specific technological demands.

Acknowledgements

The authors kindly acknowledge Prof. Dr. Eberhard Müller, Institute of Electronic and Sensor Materials, Technical University of Freiberg, for his discussion on the particle crystallization, Prof. Dr. Ute Kaiser and her team, Transmission Electron Microscopy Group of Materials Science, University of Ulm, for the TEM micrographs and the EDX elemental mapping of the zirconia–alumina composite nanoparticles, and Dr. Christiane Oestreich, Institute of Electronic and Sensor Materials, Technical University of Freiberg, for the XRD analysis and the chemical analysis of the zirconia–alumina nanopowder. They also thank Ingmar Zink, Christian Stötzel, and Alexander Conrad, Institute of Materials Science and Technology, University of Jena, for

experimental assistance. This work was partly financially supported by the Deutsche Forschungsgemeinschaft (DFG) under Grant Nos. STA 400/6 and STA 400/14.

References

1. Srdić VV, Winterer M. Comparison of nanosized zirconia synthesized by gas and liquid phase methods. *J Eur Ceram Soc* 2006;**26**(15):3145–51.
2. Tahmasebpour M, Babaluo AA, Razavi Aghjeh MK. Synthesis of zirconia nanopowders from various zirconium salts via polyacrylamide gel method. *J Eur Ceram Soc* 2008;**28**(4):773–8.
3. Raming T, Winnubst L, Verweij H. The synthesis and characterisation of mixed Y_2O_3-doped ZrO_2 and α-Fe_2O_3 nanosized powders. *J Mater Chem* 2002;**12**:3705–11.
4. Aimable A, Buscaglia MT, Buscaglia V, Bowen P. Polymer-assisted precipitation of ZnO nanoparticles with narrow particle size distribution. *J Eur Ceram Soc* 2010;**30**(2):591–8.
5. Mädler L, Kammler HK, Mueller R, Pratsinis SE. Controlled synthesis of nanostructured particles by flame spray pyrolysis. *J Aerosol Sci* 2002;**33**(2):369–89.
6. Rosner DE. Flame synthesis of valuable nanoparticles: recent progress/current needs in areas of rate laws, population dynamics, and characterization. *Ind Eng Chem Res* 2005;**44**(16):6045–55.
7. Tok AIY, Boey FYC, Zhao XL. Novel synthesis of Al_2O_3 nano-particles by flame spray pyrolysis. *J Mater Process Tech* 2006;**178**(1–3):270–3.
8. Riehemann W. Synthesis of nanoscaled powders by laser evaporation of materials. In: Gonsalves KE, Baraton MI, Singh R, Hofmann H, Chen JX, Akkara JA, editors. *Surface-controlled nanoscale materials for high-added-value applications*, vol. 501. MRS Symposium Proceedings; 1998. p. 95–102.
9. Kerber C. *Generation of nanoparticles by laser evaporation*. Aachen: Shaker; 1998.
10. Ullmann M, Friedlander SK, Schmidt-Ott A. Nanoparticle formation by laser ablation. *J Nanopart Res* 2002;**4**:499–509.
11. Tsai MH, Shen P, Chen SY. Laser ablation condensation and defect generation of $Ti_{1-x}Zr_xO_2$ nanoparticles. *J Eur Ceram Soc* 2008;**28**(8):1631–9.
12. Müller E, Oestreich C, Popp U, Michel G, Staupendahl G, Henneberg KH. Characterization of nanocrystalline oxide powders prepared by CO_2 laser evaporation. *KONA Powder Part* 1995;**13**:79–90.
13. Staupendahl G, Michel G, Eberhardt G, Müller E, Oestreich C, Vogelsberger W, et al. Production of nanosized zirconia particles by pulsed CO_2 laser evaporation. *J Laser Appl* 1999;**11**:14–20.
14. Staupendahl G, Kurland HD, Grabow J. Production of nanoscaled powders by CO_2 laser evaporation. *IEEE LEOS Newslett* 2003;**17**:3.
15. Kurland HD, Stötzel C, Grabow J, Zink I, Müller E, Staupendahl G, et al. Preparation of spherical titania nanoparticles by CO_2 laser evaporation and process-integrated particle coating. *J Am Ceram Soc* 2010;**93**:1282–9.
16. Lohbauer U, Wagner A, Belli R, Stötzel C, Hilpert A, Kurland HD, et al. Zirconia nanoparticles prepared by laser vaporization as fillers for dental adhesives. *Acta Biomater* 2010;**6**(12):4539–46.
17. Kurland HD, Grabow J, Staupendahl G, Andrä W, Dutz S, Bellemann ME. Magnetic iron oxide nanopowders produced by CO_2 laser evaporation. *J Magn Magn Mater* 2007;**311**:73–7.
18. Kurland HD, Grabow J, Staupendahl G, Müller FA, Müller E, Dutz S, et al. Magnetic iron oxide nanopowders produced by CO_2 laser evaporation – 'In situ' coating and particle embedding in a ceramic matrix. *J Magn Magn Mater* 2009;**321**:1381–5.
19. Staupendahl G, Kurland HD, Grabow J, Oestreich C, Loogk M. In-situ coating of nano-scaled ceramic powders produced by laser evaporation. In: Müller E, Oestreich C, editors. *Handling of highly dispersed powders*. Aachen: Shaker; 2004. p. 69–78.
20. Friedlander SK. *Smoke, Dust, and Haze, fundamentals of aerosol dynamics*. Oxford: University Press; 2000.
21. Ogawa K, Vogt T, Ullmann M, Johnson S, Friedlander SK. Elastic properties of nanoparticle chain aggregates of TiO_2, Al_2O_3, and Fe_2O_3 generated by laser ablation. *J Appl Phys* 2000;**87**(1):63–73.
22. Ostwald W. Studies upon the forming and changing solid bodies. *Z Phys Chem* 1897;**22**:289–330.
23. Threlfall T. Structural and thermodynamic explanations of Ostwald's Rule. *Org Process Res Dev* 2003;**7**(6):1017–27.
24. Fanchini G, McCauley JW, Niesz DE, Chhowalla M. The Role of Multiple Polytypes in Determining the Catastrophic Failure of Boron Carbide at High Shock Velocities. In: Bradby JE, Kucheyev SO, Stach EA, Swain MV, editors. Mechanisms of Mechanical Deformation in Brittle Materials, Mater Res Soc Symp Proc 1996; 904E, paper #: 0904-BB04-22.
25. Holleman AF, Wilberg N. *Inorganic chemistry*. New York: Academic Press; 2001. p. 507.
26. Weast RC. *Handbook of chemistry and physics*. Boca Raton: CRC Press; 1984. p. B-154.
27. Grant FA. Properties of rutile (titanium oxide). *Rev Mod Phys* 1959;**31**(3):646–74.
28. Salmang H, Scholze H, Telle R. *Keramik*. 7th ed. Berlin: Springer; 2007, ISBN 3-540-63273-5, p. 237.
29. Briehl H. *Chemie der Werkstoffe*. 2nd ed. Wiesbaden: Teubner; 2008, ISBN 978-3-8351-0223-1. p. 236.
30. Jayaseelan DD, Rani DA, Nishikawa T, Awaji H, Gnanam FD. Powder characteristics, sintering behavior and microstructure of sol–gel derived ZTA composites. *J Eur Ceram Soc* 2000;**20**(3):267–75.
31. Tuan WH, Chen RZ, Wang TC, Cheng CH, Kuo PS. Mechanical properties of Al_2O_3/ZrO_2 composites. *J Eur Ceram Soc* 2002;**22**(16):2827–33.
32. Sarraf H, Herbig R, Maryška M. Fine-grained Al_2O_3–ZrO_2 composites by optimization of the processing parameters. *Scripta Mater* 2008;**59**(2):155–8.
33. Kim S, Ehrman SH. Capillary condensation onto titania (TiO_2) nanoparticle agglomerates. *Langmuir* 2007;**23**:2497–504.